ADVANCED MATERIALS INTERFACES
www.advmatinterfaces.de

Check for updates

Laser-Assisted Thermomechanical Thinning of $MoTe_2$ in Nanoscale Lateral Resolution

*Yoonsoo Rho, Hyungjin Kim, Ali Javey, and Costas P. Grigoropoulos**

A key feature of 2D transition metal dichalcogenides (2D-TMDCs) is that their properties are strongly dependent on their thickness, typically appearing in ultrathin mono- or few- layers. Thus, precise control of functional nanostructure is critical for fundamental research and applications in 2D-TMDCs. Here, atomic layer precision thinning of molybdenum ditelluride ($MoTe_2$) at nanoscale lateral resolution by introducing laser irradiated hot tip is demonstrated. The contact of the hot tip on $MoTe_2$ surface promotes oxidation at nanoscale resolution which is simultaneously removed by thermomechanical scribing. This process completes the atomic layer precision thinning of $MoTe_2$ while maintaining the high crystallinity of thinned $MoTe_2$ flake. Further, the electrical properties of the $MoTe_2$ flake are intact after thinning, which proves that the thinned $MoTe_2$ flake obtained by these methods can potentially be utilized for device fabrication. It is believed that the work will enable applications of 2D-TMDCs that require nanoscale resolution with controlled thickness.

1. Introduction

A unique range of properties of atomically thin TMDC semiconductors strongly depend on their thickness, and typically appear in ultrathin mono- or few- layers. The reduced physical dimension of TMDCs renders confined 2D electron profiles, thereby enabling relatively large direct band gap (1.1 eV ≈ 1.8 eV),[1] rich excitonic dynamics,[2] and various nonlinear optical properties,[3,4] while exhibiting high on/off ratio and moderately high mobility up to (200 $cm^2 V^{-1} s$ at room temperature).[5,6] On the other hand, precise control of thickness at nanoscale lateral resolution could foster various nanoscale applications by taking virtue of thickness-dependent optoelectronic properties of TMDCs, for instance in nanoscale optical gratings and electronic band modulations. Layers of reduced thickness that are relatively free of defects could realize high-density functional devices with reduced power consumption.[7]

Despite those advantages, the technological advancement in defining the thickness of TMDCs in nanoscale lateral resolution is still rudimentary. Conventionally, TMDC thickness control has been demonstrated by plasma etching,[8,9] thermal or chemical etching by furnace[10,11] or laser heating.[12–14] However, those methods possess drawbacks, including significant defect formation introduced by energetic particles or high temperature, contamination by incorporation of wet lithography process for defining nano features, and low lateral resolution imposed by optical diffraction limits, respectively. Alternatively, tip-based scanning probe lithography (SPL) methods have been considered as promising for manipulation of functional nanostructures[15] by introducing local heating,[16–19] chemical reactions,[20–22] or mechanical scratching.[23] Among various tip-based SPLs, the lightning rod effect by laser illumination at the plasmonic tip apex was first studied, inducing local heating by field enhancement.[16] On the other hand, the tip temperature can be raised by joule heating[15,18] or under laser illumination,[19] providing locally confined heat source to the sample surface upon contact with hot tip. These thermal approaches are advantageous over other SPLs that apply charged particles such as electrons or ions which can be detrimental to the properties of the processed 2D layers.[18] Recently, Liu et al. have shown patterning and deformation of TMDC materials transferred on polymer thin films using electrically heated hot tip.[24,25] However, the atomic layer precision thinning of TMDCs would be difficult to achieve using this method due to the thermally and mechanically vulnerable polymer sublayer. The thinning process requires thermally activated chemical reaction on top layer that should be subsequently removed by either thermal evaporation or physical removal, while the maximum induced temperature and mechanical force should be kept below the damage threshold of the sublayer. In addition, the joule heating with a complicated electrical circuit design limits the choice of the mechanical properties and functional coating materials of the tip that could be critical for the thinning process of TMDC materials.

Here, we introduce a laser-heated tip for atomic layer precision thinning of $MoTe_2$ with nanoscale lateral resolution. The

Y. Rho, C. P. Grigoropoulos
Laser Thermal Laboratory
Department of Mechanical Engineering
University of California
Berkeley, California 94720, USA
E-mail: cgrigoro@berkeley.edu
H. Kim, A. Javey
Laboratory for Materials and Device Innovation
Department of Electrical Engineering and Computer Sciences
University of California
Berkeley, California 94720, USA

The ORCID identification number(s) for the author(s) of this article can be found under https://doi.org/10.1002/admi.202200634.

DOI: 10.1002/admi.202200634

© 2022 Wiley-VCH GmbH

21967350, 2022, 23, Downloaded from https://onlinelibrary.wiley.com/doi/10.1002/admi.202200634 by Univ of California Lawrence Berkeley National Lab, Wiley Online Library on [11/01/2023]. See the Terms and Conditions (https://onlinelibrary.wiley.com/terms-and-conditions) on Wiley Online Library for rules of use; OA articles are governed by the applicable Creative Commons License

laser heating method allows the use of conventional silicon tip to rapidly control the induced temperature in $MoTe_2$ surface. The contact of heated hot tip oxidizes the $MoTe_2$ top layer, and the scribing of the hot tip with mechanical indentation force thermo-mechanically removes the oxidized top layer. This process results in atomic layer precision thinning in nanoscale lateral resolution, while maintaining high crystallinity of $MoTe_2$. In addition, the thinned $MoTe_2$ flake maintains its electric transport properties, which proves that our newly developed thinning process would enable various nanoscale applications based on TMDC materials.

2. Results and Discussion

Figure 1a shows schematics of the thinning of TMDCs by laser-heated hot tip. For the TMDC sample, we chose $MoTe_2$ as its low electronegativity difference between Mo and Te ($\Delta\chi \approx 0.3$)[26,27] renders relatively low oxidation temperature (≈470 K[28]), which justifies its choice as TMDC material for exploring our new processing method. The $MoTe_2$ flake was prepared by mechanical exfoliation on SiO_2/Si substrate. For the processing, we implemented a femtosecond laser beam ($\lambda \approx 800$ nm, f ≈ 80 MHz, pulse duration ≈100 fs, focal spot size ≈10 μm), as we first explored the possibility of noncontact nanomachining by utilizing the "lightning rod effect" upon illuminating ultrafast pulses at the metallic tip apex (Supplementary Note 1). However, the floating tip operating in a non-contact mode could not efficiently remove the formed oxides. This limitation forced us to rely on thermomechanical thinning by scribing with a laser-heated hot tip as described in Figure 1b,c.

We found that the pulsed laser at a high repetition rate can act as quasi-continuous heat source when illuminated at the tip, which rendered steady-state temperature at the tip apex. The laser-heated hot tip contacted the surface of the target specimen, providing nanoscale localized heat source supplemented with mechanical force to remove the formed oxides. Once the local temperature of $MoTe_2$ exceeded the oxidation temperature of $MoTe_2$, the top-most layer of the flake reacted with ambient oxygen, possibly forming TeO_x and MoO_3. It has been reported that in the blanket annealing process (i.e., furnace annealing), the oxides remained at the top surface of $MoTe_2$ without evaporation due to the high boiling temperature of TeO_x (1005 K).[28] In our experiment, we observed an etched pit with bump shape upon contact of laser-heated silicon tip on $MoTe_2$ surface (Figure 1d). The width of the etched area was ≈20 nm as shown

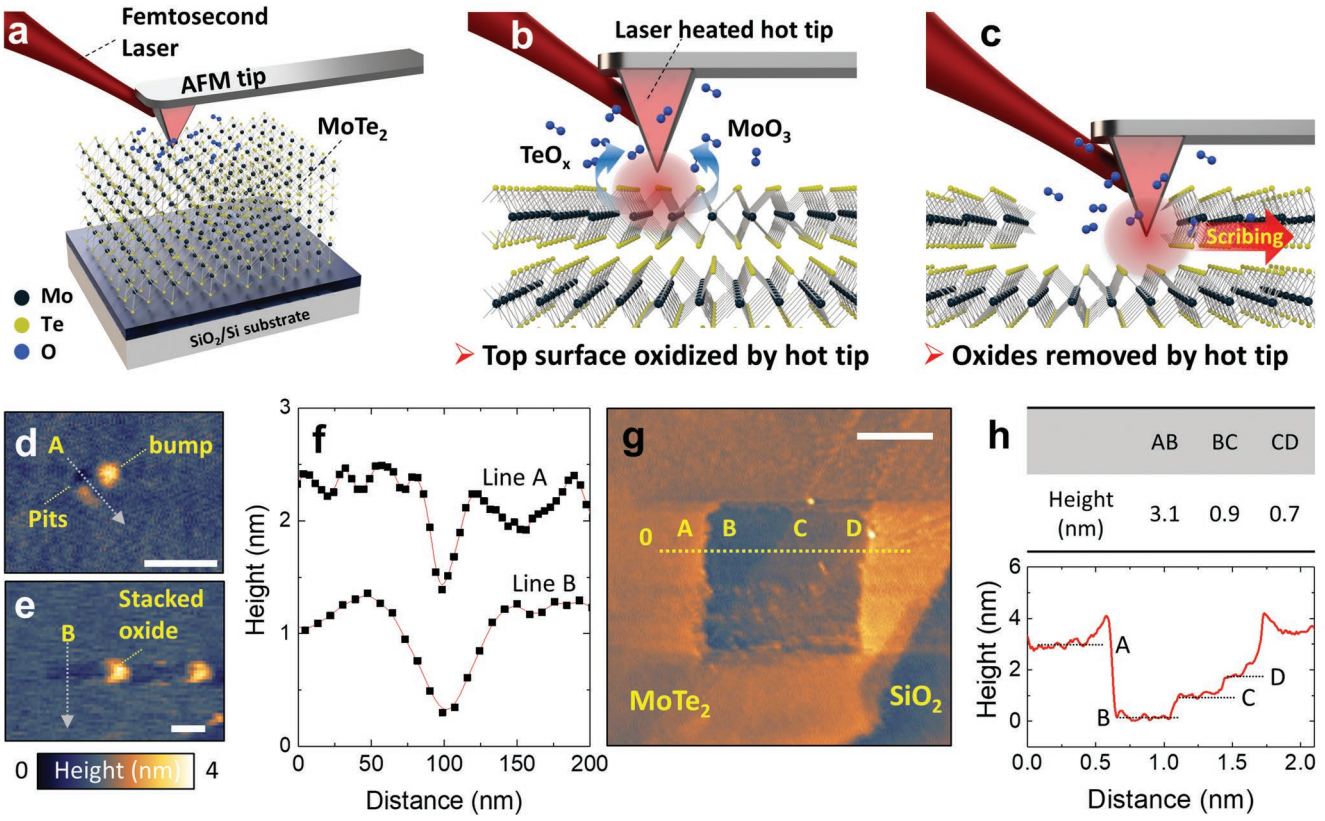

Figure 1. a) Schematics of nanoscale thinning of $MoTe_2$ exfoliated on SiO_2/Si substrate using laser-heated hot tip. b) The illustration of the top layer oxidized by contact hot tip under the ambient condition, and c) the illustration of simultaneous scribing of hot tip to remove the oxidized top layer of $MoTe_2$. Topography images of $MoTe_2$ after d) initial contact and e) scribing of hot tip. The scale bars in d) and e) indicate 100 nm. f) Line profiles of $MoTe_2$ surface along the lines A and B indicated in panels d-e), which show 20 nm and 55 nm of widths and 0.9 nm of depths indicating monolayer thinning in nanoscale resolution. g) Topography image of $MoTe_2$ flake after performing hot tip-induced thinning process. The scale bar indicates 1 μm. h) Line profile along the line in panel g) showing the thickness differences between the points B and C, and the points C and D are 0.9 and 0.7 nm, respectively, which implies that the monolayer thickness difference was preserved during the thinning process.

© 2022 Wiley-VCH GmbH

21967350, 2022, 23, Downloaded from https://onlinelibrary.wiley.com/doi/10.1002/admi.202200634 by Univ of California Lawrence Berkeley National Lab, Wiley Online Library on [11/01/2023]. See the Terms and Conditions (https://onlinelibrary.wiley.com/terms-and-conditions) on Wiley Online Library for rules of use; OA articles are governed by the applicable Creative Commons License

21967350, 2022, 23, Downloaded from https://onlinelibrary.wiley.com/doi/10.1002/admi.202200634 by Univ of California Lawrence Berkeley National Lab, Wiley Online Library on [11/01/2023]. See the Terms and Conditions (https://onlinelibrary.wiley.com/terms-and-conditions) on Wiley Online Library for rules of use; OA articles are governed by the applicable Creative Commons License

in Figure 1f, which is comparable to the diameter of the tip, while the bump observed in the vicinity of the pit was due to the oxidation of the top surface. Then, the scribing of the hot tip on $MoTe_2$ surface resulted in local removal of the top-most layer and the formation of stacked oxides (Figure 1e). Also, the depths of both etched pit and thinned area were 0.9 nm, which is close to the monolayer thickness of $MoTe_2$. Meanwhile, the measured 55 nm width of the thinned line was larger than the diameter of the pristine tip (Figure 1f). We attribute this to increased tip diameter due to the tip degradation by the large contact force (Supplementary Note 3). Figure 1g,h show uniform thickness removal on multi-step structure of $MoTe_2$, maintaining 0.9 nm and 0.7 nm height differences between the lines B and C, and C and D, respectively. This result indicates that the thinning process preserved the monolayer thickness difference after the thinning process.

Depending on the illuminated laser power, the thickness of $MoTe_2$ flake can be controlled with atomic layer precision. As shown in **Figure 2**a–d, we started from penta-layer. The laser power for heating the tip was varied from 50 to 80 mW, while the hot tip was raster scanned over 2 μm by 2 μm of square area for three times. We performed large area thinning for the optical diagnostics including Raman and second harmonic generation (SHG) whose resolutions are limited in micrometer scale by optical diffraction. The speed of scribing of the hot tip was kept at 0.4 μm sec^{-1} with 15 nm gap between the lines, resulting 0.36 μm^2 min^{-1} of area processing speed. After the thinning processes, the colors of thinned regions clearly changed depending on the thickness of thinned $MoTe_2$. The line profiles obtained from the thinned flakes by AFM measurement showed quad- tri-, bi-, and mono-layer thicknesses (insets of Figure 2a–d). Raman spectra using laser excitation at 532 nm exhibited clear changes in their B_{2g} and $E_{2g}{}^1$ peak intensities after the thinning process, while all pristine and thinned flakes indicate 2H phase $MoTe_2$ (Figure 2h). Raman spectra of pristine 2H-$MoTe_2$ upon 532 nm excitation show clear features depending on thickness.[29] The thinner the $MoTe_2$ flake, the higher the peak intensity ratio between B_{2g} and $E_{2g}{}^1$ peaks ($I_{B_{2g}}/I_{E^1_{2g}}$) should be observed, except for monolayer where B_{2g} intensity abruptly drops. The thinned $MoTe_2$ flake by our method also showed the same trend, indicating layer controlled thinning process. The $I_{B_{2g}}/I_{E^1_{2g}}$ mapping image obtained from Figure 2a showed clear enhancement over the thinned region (Figure 2g). Previous reports observed phase transition of $MoTe_2$ from 2H to 1T' by laser thinning, which was attributed to the lattice pinning due to the defect formation by laser ablation process.[30] However, there was no evidence of phase transition in our experimental results. Further, the azimuthal angle plot of optical SHG obtained from the thinned area proved the high crystallinity of the thinned flake without phase transition as shown in Figure 2e. The clear sixfold symmetricity observed from the thinned $MoTe_2$ implies high-quality 2H phase crystalline structure,[3] whereas 1T' phase should exhibit a butterfly shape.[31]

To estimate the induced temperature at the tip apex by laser heating, we obtained the relation between the tip temperature by laser heating and the resonance frequency of the tip, based on heat transfer and solid mechanics simulations (Supplementary

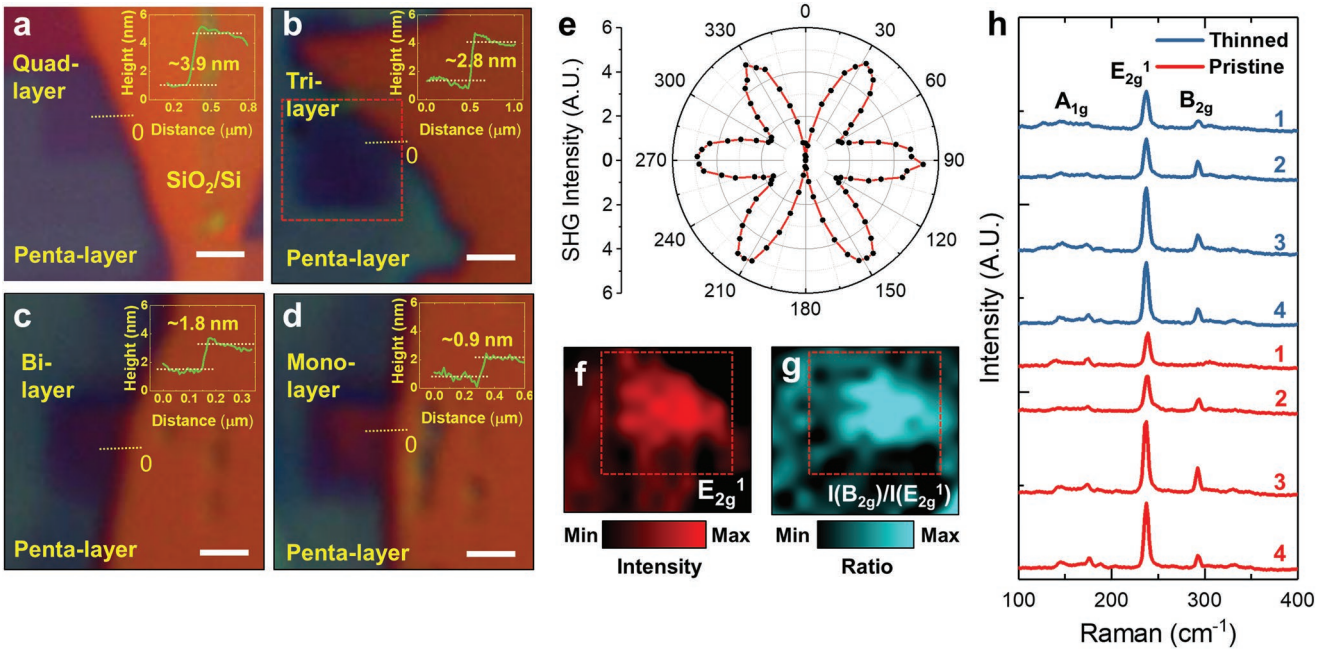

Figure 2. Demonstration of atomic layer precision thinning of $MoTe_2$ by laser-heated hot tip. a–d) Microscope images and AFM line profiles (insets) along the dashed lines showing a large area (2 μm by 2 μm) thinning of penta-layer $MoTe_2$ flakes by thermomechanical thinning process, resulting in a) quad-layer, b) tri-layer, c) bi-layer, and d) mono-layer thinned area. The scale bars indicate 1 μm. e) Angle-resolved second harmonic generation (SHG) plot obtained from the tri-layer thinned region in panel b), showing six-fold symmetricity, manifesting preserved crystalline structure of 2H-phase $MoTe_2$ after the thinning process. f–g) Raman $E_{2g}{}^1$ peak intensity and peak intensity ratio ($I_{B_{2g}}/I_{E^1_{2g}}$) mapping images obtained from the red-dashed box in panel b). h) Raman spectra obtained from the pristine (blue) and thinned (red) quad-, tri-, bi-, and mono-layer $MoTe_2$ flakes, indicated by the numbers in the right side.

© 2022 Wiley-VCH GmbH

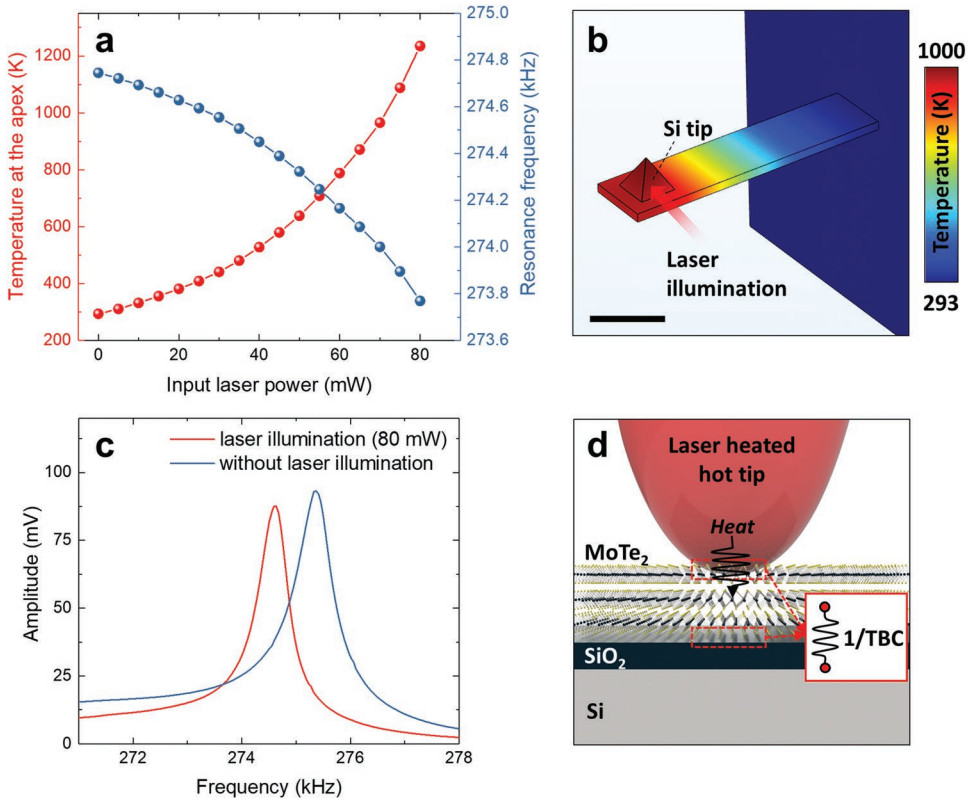

Figure 3. Heat transfer and solid mechanics simulation of the tip under the illumination of the laser beam at the tip body. a) Calculated temperatures at the tip apex and corresponding mechanical resonance frequencies depending on the input laser power. b) 3D temperature profile of the tip under the illumination of the laser at 80 mW of power. The scale bar indicates 50 µm. c) Experimentally measured frequency response of the amplitude of the tip with and without laser illumination of 80 mW. d) Schematical illustration of the heated hot tip in contact with the surface of $MoTe_2$ on SiO_2/Si wafer with the thermal boundary conductance (TBC) of the $MoTe_2$/Si tip and $MoTe_2$/SiO_2 substrate interfaces.

Note 5). Here, we modeled the laser heating as a quasi-continuous heat source, due to the use of the high repetition rate (80 MHz) of laser pulse trains and the low heat dissipation through the cantilever body that rendered the heat transfer approximately one-dimensional. In addition, despite the long optical penetration depth (≈10 µm) of silicon at 800 nm, the strong multiphoton absorption effect of silicon by femtosecond pulse enhanced the absorption of laser power. The simulation result showed that the temperature of the tip apex can reach 1230 K at steady-state under the illumination of 80 mW laser power (**Figure 3**a). Meanwhile, due to the resulted nonuniform temperature distribution through the cantilever and the temperature-dependent Young's modulus of silicon,[32] the solid mechanics simulation showed the downshift of the mechanical resonance frequency of the tip from 274.74 to 273.89 kHz. The experimentally observed drop in resonance frequency upon the laser illumination of 80 mW was ≈0.8 kHz, which corresponds to ≈1200 K of the temperature of the tip apex (Figure 3c).

Despite such high temperature of the tip, our nanoscale thinning process maintained the high crystallinity of the thinned flake as shown in SHG and Raman studies (Figure 2), indicating a large temperature difference between the tip and the $MoTe_2$. We expect that the induced temperature at $MoTe_2$ should be high enough for oxidation (≈470 K[28]), but smaller than the thermal decomposition temperature of $MoTe_2$ (≈670 K[28]). The abrupt temperature drop can be ascribed to the low thermal boundary conductance (TBC) at the interface between TMDC materials and bulk flat substrate as illustrated in Figure 3d due to the limited coupling of flexural phonon mode of TMDCs with bulk substrates.[33,34] In addition, the nanoscale heat source provided by the tip apex could result in a larger temperature drop due to the 3D heat diffusion. However, we should note that the TBC in our experiment was hard to estimate as it could be readily altered by surface chemistry, roughness, and pressure[18] during the thinning process. Further studies would be required for a better understanding of the heat transfer at the interface.

The $MoTe_2$ flake obtained by the thinning process maintained its electrical properties, which was investigated based on $MoTe_2$ field-effect transistor (FET) devices. The pristine $MoTe_2$ flake on SiO_2 (50 nm)/Si was patterned to a strip shape by lithography and channels were fabricated by deposition of metal electrode. Source drain current (I_d) curves were obtained while back gate voltage (V_g) was swept from −20 V to 20 V, which showed p-type behavior (**Figure 4**a). The thinning process was performed on $MoTe_2$ channel area. After the hot tip induced thinning process, the thickness decreased by ≈1–2 nm according to the line profiles in Figure 4b. I_d-V_g curve obtained after the thinning process yielded current level and on-off ratio comparable to the results from the flake prior to the thinning process, as shown in Figure 4a. Hence, the remaining $MoTe_2$ flake after the thinning process was not damaged and kept its electrical performance

© 2022 Wiley-VCH GmbH

21967350, 2022, 23, Downloaded from https://onlinelibrary.wiley.com/doi/10.1002/admi.202200634 by Univ of California Lawrence Berkeley National Lab, Wiley Online Library on [11/01/2023]. See the Terms and Conditions (https://onlinelibrary.wiley.com/terms-and-conditions) on Wiley Online Library for rules of use; OA articles are governed by the applicable Creative Commons License

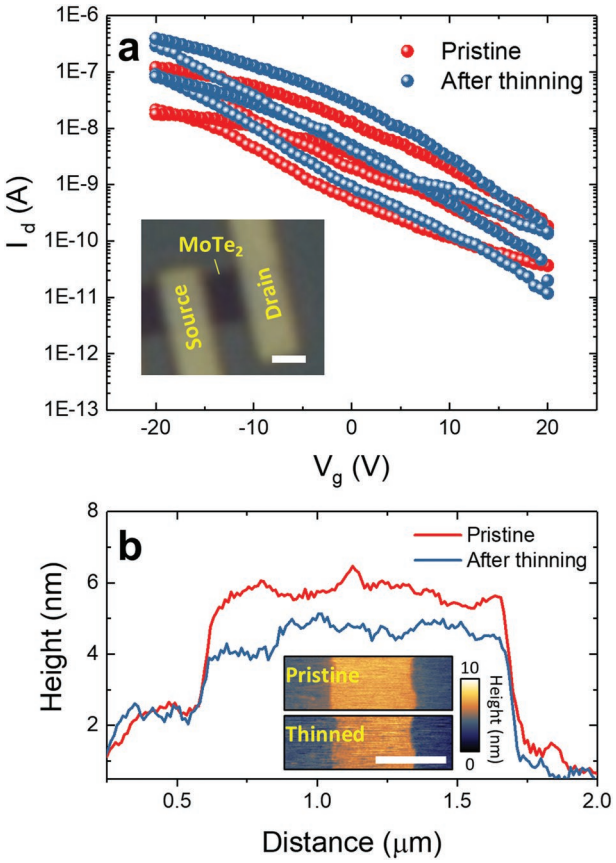

Figure 4. Demonstration of the effect of hot tip-induced thinning process on electrical properties of $MoTe_2$ based on field-effect transistor (FET) device. a) Drain current (I_d) -gate voltage (V_g) curves of $MoTe_2$ FET device obtained from before and after thinning process. The inset image shows an optical microscope image of the $MoTe_2$ FET device. The scale bar indicates 1 μm. b) topography line profiles and topography images (inset) of $MoTe_2$ FET device before and after thinning process. The scale bars indicate 1 μm.

characteristics, confirming that our developed thermomechanical nanothinning process can be applied in the fabrication of various nanoscale device applications.

3. Conclusion

We demonstrated atomic layer precision thinning of $MoTe_2$ in nanoscale lateral resolution by laser-assisted thermomechanical thinning process. Raman and SHG analysis showed that the thinned flake maintained high crystallinity with minimal damage. We attribute this process to the oxidation of $MoTe_2$ promoted by the hot tip contact, and the subsequent removal process by thermomechanical scribing. Heat transfer and solid mechanics simulations as well as the tip resonance frequency measurement upon the laser illumination confirmed that high steady-state temperature can be induced at the tip apex. More importantly, the electrical performance characterization revealed enhanced current level and on-off ratio, manifesting high-quality thinned $MoTe_2$ flake. We believe that the presented nanoscale thinning process is applicable to other TMDC materials and will enable future nanoscale device applications.

4. Experimental Section

Thinning Process: The thinning process was performed based on Molecular Vista (Vistascope) AFM system. A Ti:sapphire femtosecond laser (Tsunami, Spectra Physics, $\lambda \approx 800$ nm, $f \approx 80$ MHz, pulse duration ≈100 fs) was utilized. For the noncontact mode processing (lightening rod effect), the laser beam was focused on the Pt-coated Si tip (PPP-NCHPt, Nanosensors) apex. For the contact mode thermomechanical process, the laser beam was focused on the side of the uncoated PPP-NCH Si tip with ≈45 N m^{-1} of spring constant. The top surface of the cantilever was coated with Pt film to improve the reflectivity for positioning of the cantilever. Then, the thinning process was performed by the contact scanning mode with 360 nN ≈ 720 nN of contact force (Supplementary Note 2).

Materials and Characterization: 2H-$MoTe_2$ flake was mechanically exfoliated on SiO_2 (300 nm)/Si wafer. For Raman study, commercial Raman system (inVia, Renishaw) was utilized with a CW 532 nm laser focused by a 100X objective lens and 1800 cm^{-1} grating. Details of SHG measurement are in Supplementary Note 4.

Device Fabrication: The mechanically exfoliated $MoTe_2$ flake on SiO_2 (50 nm)/Si wafer was defined in its shape using electron beam lithography (EBL) using PMMA (Poly (methyl methacrylate), MicroChem) as a positive resist, followed by XeF_2 etching to remove the area outside the channel. The metal electrode was subsequently patterned by the same EBL process with Cr/Au electrode (5/30 nm) formed by evaporation and lift-off process.

Heat Transfer and Solid Mechanics Simulation: Details of heat transfer and solid mechanics simulation are described in Supplementary Note 5.

Supporting Information

Supporting Information is available from the Wiley Online Library or from the author.

Acknowledgements

Y.R. and H.K. contributed equally to this work. Financial support awarded to the University of California, Berkeley, by the U.S. National Science Foundation (Grant No. CMMI-2024391) is gratefully acknowledged. The COMSOL simulation was performed at the Molecular Graphics and Computation Facility, University of California, Berkeley, funded by NIH S10OD023532.

Conflict of Interest

The authors declare no conflict of interest.

Data Availability Statement

The data that support the findings of this study are available from the corresponding author upon reasonable request.

Keywords

2D materials, atomic layer precision thinning, laser-irradiated hot tip, $MoTe_2$, nanoscale process

Received: March 21, 2022
Revised: May 22, 2022
Published online: July 13, 2022

© 2022 Wiley-VCH GmbH

21967350, 2022, 23, Downloaded from https://onlinelibrary.wiley.com/doi/10.1002/admi.202200634 by Univ of California Lawrence Berkeley National Lab, Wiley Online Library on [11/01/2023]. See the Terms and Conditions (https://onlinelibrary.wiley.com/terms-and-conditions) on Wiley Online Library for rules of use; OA articles are governed by the applicable Creative Commons License

[1] F. Xia, H. Wang, D. Xiao, M. Dubey, A. Ramasubramaniam, *Nat. Photonics* **2014**, *8*, 899.
[2] K. F. Mak, C. Lee, J. Hone, J. Shan, T. F. Heinz, *Phys. Rev. Lett.* **2010**, *105*, 136805.
[3] L. M. Malard, T. V. Alencar, A. P. M. Barboza, K. F. Mak, A. M. de Paula, *Phys. Rev. B* **2013**, *87*, 201401.
[4] Y. Li, Y. Rao, K. F. Mak, Y. You, S. Wang, C. R. Dean, T. F. Heinz, *Nano Lett.* **2013**, *13*, 3329.
[5] X. Cui, G.-H. Lee, Y. D. Kim, G. Arefe, P. Y. Huang, C.-H. Lee, D. A. Chenet, X. Zhang, L. Wang, F. Ye, F. Pizzocchero, B. S. Jessen, K. Watanabe, T. Taniguchi, D. A. Muller, T. Low, P. Kim, J. Hone, *Nat. Nanotechnol.* **2015**, *10*, 534.
[6] S. Kim, A. Konar, W.-S. Hwang, J. H. Lee, J. Lee, J. Yang, C. Jung, H. Kim, J.-B. Yoo, J.-Y. Choi, Y. W. Jin, S. Y. Lee, D. Jena, W. Choi, K. Kim, *Nat. Commun.* **2012**, *3*, 1011.
[7] M. Lundstrom, *IEEE Electron Device Lett.* **1997**, *18*, 361.
[8] Y. Liu, H. Nan, X. Wu, W. Pan, W. Wang, J. Bai, W. Zhao, L. Sun, X. Wang, Z. Ni, *ACS Nano* **2013**, *7*, 4202.
[9] K. S. Kim, K. H. Kim, Y. Nam, J. Jeon, S. Yim, E. Singh, J. Y. Lee, S. J. Lee, Y. S. Jung, G. Y. Yeom, D. W. Kim, *ACS Appl. Mater. Interfaces* **2017**, *9*, 11967.
[10] M. Yamamoto, T. L. Einstein, M. S. Fuhrer, W. G. Cullen, *J. Phys. Chem. C* **2013**, *117*, 25643.
[11] H. Zhou, F. Yu, Y. Liu, X. Zou, C. Cong, C. Qiu, T. Yu, Z. Yan, X. Shen, L. Sun, B. I. Yakobson, J. M. Tour, *Nano Res.* **2013**, *6*, 703.
[12] Y. Rho, J. Pei, L. Wang, Z. Su, M. Eliceiri, C. P. Grigoropoulos, *ACS Appl. Mater. Interfaces* **2019**, *11*, 39385.
[13] A. Castellanos-Gomez, M. Barkelid, A. M. Goossens, V. E. Calado, H. S. J. van der Zant, G. A. Steele, *Nano Lett.* **2012**, *12*, 3187.
[14] V. K. Nagareddy, T. J. Octon, N. J. Townsend, S. Russo, M. F. Craciun, C. D. Wright, *Adv. Funct. Mater.* **2018**, *28*, 1804434.
[15] R. Garcia, A. W. Knoll, E. Riedo, *Nat. Nanotechnol.* **2014**, *9*, 577.
[16] A. Chimmalgi, D. J. Hwang, C. P. Grigoropoulos, *Nano Lett.* **2005**, *5*, 1924.
[17] D. Hwang, S.-G. Ryu, N. Misra, H. Jeon, C. P. Grigoropoulos, *Appl. Phys. A* **2009**, *96*, 289.
[18] S. T. Howell, A. Grushina, F. Holzner, J. Brugger, *Microsyst. Nanoeng.* **2020**, *6*, 21.
[19] A. A. Milner, K. Zhang, Y. Prior, *Nano Lett.* **2008**, *8*, 2017.
[20] P. Zhao, R. Wang, D.-H. Lien, Y. Zhao, H. Kim, J. Cho, G. H. Ahn, A. Javey, *Adv. Mater.* **2019**, *31*, 1900136.
[21] Y. K. Ryu, R. Garcia, *Nanotechnology* **2017**, *28*, 142003.
[22] Z. Wei, D. Wang, S. Kim, S.-Y. Kim, Y. Hu, M. K. Yakes, A. R. Laracuente, Z. Dai, S. R. Marder, C. Berger, W. P. King, W. A. de Heer, P. E. Sheehan, E. Riedo, *Science* **2010**, *328*, 1373.
[23] G. Lu, X. Zhou, H. Li, Z. Yin, B. Li, L. Huang, F. Boey, H. Zhang, *Langmuir* **2010**, *26*, 6164.
[24] X. Liu, A. K. Sachan, S. T. Howell, A. Conde-Rubio, A. W. Knoll, G. Boero, R. Zenobi, J. Brugger, *Nano Lett.* **2020**, *20*, 8250.
[25] X. Liu, S. T. Howell, A. Conde-Rubio, G. Boero, J. Brugger, *Adv. Mater.* **2020**, *32*, 2001232.
[26] F. R. Gamble, *J. Solid State Chem.* **1974**, *9*, 358.
[27] G. Mirabelli, C. McGeough, M. Schmidt, E. K. McCarthy, S. Monaghan, I. M. Povey, M. McCarthy, F. Gity, R. Nagle, G. Hughes, A. Cafolla, P. K. Hurley, R. Duffy, *J. Appl. Phys.* **2016**, *120*, 125102.
[28] L. Yang, H. Wu, W. Zhang, Z. Chen, J. Li, X. Lou, Z. Xie, R. Zhu, H. Chang, *Nanoscale* **2018**, *10*, 19906.
[29] C. Ruppert, O. B. Aslan, T. F. Heinz, *Nano Lett.* **2014**, *14*, 6231.
[30] S. Cho, S. Kim, J. H. Kim, J. Zhao, J. Seok, D. H. Keum, J. Baik, D.-H. Choe, K. J. Chang, K. Suenaga, S. W. Kim, Y. H. Lee, H. Yang, *Science* **2015**, *349*, 625.
[31] R. Beams, L. G. Cançado, S. Krylyuk, I. Kalish, B. Kalanyan, A. K. Singh, K. Choudhary, A. Bruma, P. M. Vora, F. Tavazza, A. V. Davydov, S. J. Stranick, *ACS Nano* **2016**, *10*, 9626.
[32] J. Vanhellemont, A. K. Swarnakar, O. V. der Biest, *ECS Trans.* **2014**, *64*, 283.
[33] E. Yalon, Ö. B. Aslan, K. K. H. Smithe, C. J. McClellan, S. V. Suryavanshi, F. Xiong, A. Sood, C. M. Neumann, X. Xu, K. E. Goodson, T. F. Heinz, E. Pop, *ACS Appl. Mater. Interfaces* **2017**, *9*, 43013.
[34] C. Monachon, L. Weber, C. Dames, *Annu. Rev. Mater. Res.* **2016**, *46*, 433.

© 2022 Wiley-VCH GmbH

21967350, 2022, 23, Downloaded from https://onlinelibrary.wiley.com/doi/10.1002/admi.202200634 by Univ of California Lawrence Berkeley National Lab, Wiley Online Library on [11/01/2023]. See the Terms and Conditions (https://onlinelibrary.wiley.com/terms-and-conditions) on Wiley Online Library for rules of use; OA articles are governed by the applicable Creative Commons License